Crystal Growth, Structural, and Property Studies on a Family of Ternary Rare-Earth Phases RE_2InGe_2 (RE = Sm, Gd, Tb, Dy, Ho, Yb)

Paul H. Tobash, Daniel Lins, and Svilen Bobev*

Department of Chemistry and Biochemistry, University of Delaware, Newark, Delaware 19716

Ana Lima, Michael F. Hundley, Joe D. Thompson, and John L. Sarrao

Materials Science and Technology Division, Los Alamos National Laboratory, Los Alamos, New Mexico 87545

Received July 23, 2005. Revised Manuscript Received August 26, 2005

A series of new rare-earth indium−germanides RE_2InGe_2 (RE = Sm, Gd, Tb, Dy, Ho, Yb) have been prepared from the corresponding elements through high-temperature reactions using an excess of indium as flux. Single-crystal and powder X-ray diffraction studies showed that these ternary phases crystallize in the tetragonal space group *P*4/*mbm*, $Z = 2$, Pearson's symbol tP10, and represent new members of the Mo_2FeB_2 family (an ordered ternary variant of the U_3Si_2 structure type). The temperature dependence of the dc magnetization (5−300 K) indicates that the RE_2InGe_2 (RE = Sm−Ho) compounds order magnetically below ca. 60 K, whereas Yb_2InGe_2 exhibits Pauli-like temperature-independent paramagnetism. Isothermal magnetization, electrical resistivity, and calorimetry measurements are presented as well and confirm the existence of ordered antiferromagnetic states at low temperatures. The structural trends and the evolution of the magnetic properties are also discussed.

Introduction

Interest in the study of non-cuprate superconductors has increased remarkably in recent years, inspired mainly from their rich structural variety and the lack of a rationale to predict new superconductors, either with previously known or unknown structures.[1−6] The unexpected discovery of superconductivity at 39 K in the long known binary compound MgB_2[7] further fueled speculations that many interesting physical properties are favored when the electron mobility is limited to fewer than three dimensions[8] and attracted much attention to other binary compounds within the prominent AlB_2 family.

Some of these efforts have proven successful; for instance, application of external pressure makes the puckered Si_2^{2-} layers in $CaSi_2$ flat, and the material becomes superconductive with T_c of 14 K.[9] It has been shown that a similar effect could also be achieved by small changes in the crystallographic and electronic environment of the Ca cation due to substitution with Ga in the Si sublattice.[10] Ga-doped $Ca(Ga_xSi_{1-x})_2$ phase has the AlB_2 structure and loses resistance at ambient pressure, although the critical temperature is not as high, ca. 3.5 K. Discoveries and studies of other structurally related intermetallic compounds are therefore relevant to the better understanding of the origins of such phenomena and motivated this work.

*R*are-*e*arth (RE) gallides, silicides, and germanides also contain compounds with the AlB_2 structure type.[11] These are formed predominantly with the metals from the second half of the lanthanide family, and in most cases, the ideal 1:2 composition is rarely realized. Various, almost exclusively $REGe_{2-x}$ substoichiometric compounds abound, where partial or full ordering of the vacancies often gives rise to novel superstructures.[12] The number of new AlB_2-based derivatives continues to grow and appears far from being exhausted.[13] Intrigued by the superconductivity in MgB_2 and by the rich phenomenology of the structurally related rare-earth ger-

* Corresponding author. Phone: (302) 831-8720. Fax: (302) 831-6335. E-mail: sbobev@chem.udel.edu.

(1) Stephens, P. W.; Mihaly, L.; Lee, P. L.; Whetten, R. L.; Huang, S. M.; Kaner, R.; Deiderich, F.; Holczer, K. *Nature* **1991**, *351*, 6328.
(2) Kawaji, H.; Horie, H.; Yamanaka, S.; Ishikawa, M. *Phys. Rev. Lett.* **1995**, *74*, 1427.
(3) Maeno, Y.; Hashimoto, H.; Yoshida, K.; Nishizaki, S.; Fujita, T.; Bednorz, J. G.; Lichtenberg, F. *Nature* **1994**, *372*, 6506.
(4) Takada, K.; Sakurai, H.; Takayama-Muromachi, E.; Izumi, F.; Dilanian, R. A.; Sasaki, T. *Nature* **2003**, *422*, 53.
(5) Henn, R. W.; Schnelle, W.; Kremer, R. K.; Simon, A. *Phys. Rev. Lett.* **1996**, *77*, 374.
(6) Tou, H.; Maniwa, Y.; Koiwasaki, T.; Yamanaka, S. *Phys. Rev. Lett.* **2001**, *86*, 5775.
(7) Nagamatsu, J.; Nakagawa, N.; Muranaka, T.; Zenitani, Y.; Akimitsu, J. *Nature* **2001**, *410*, 6824.
(8) King, R. B. In *Concepts in Chemistry*; Rouvray, D. H., Ed.; Wiley: New York, 1997.
(9) Sanfilippo, S.; Elsinger, H.; Nunez-Regueiro, M.; Laborde, O.; LeFloch, S.; Affronte, M.; Olcese, G. L.; Palenzona, A. *Phys. Rev. B* **2000**, *61*, R3800.
(10) Imai, M.; Nishida, K.; Kimura, T.; Abe, H. *Physica C* **2002**, *377*, 96.
(11) Villars, P.; Calvert, L. D. (Eds.) *Pearson*'s Handbook of Crystallographic Data for Intermetallic Compounds, 2nd ed.; American Society for Metals: Metals Park, OH, 1991.
(12) a) Venturini, G.; Ijjaali, I.; Malaman, B. *J. Alloys Compd.* **1999**, *285*, 194. (b) Schobinger-Papamantellos, P.; De Mooij, D. B.; Buschow, K. H. J. *J. Less-Common Met.* **1990**, *163*, 319.
(13) a) Venturini, G.; Ijjaali, I.; Malaman, B. *J. Alloys Compd.* **1999**, *284*, 262. (b) Oleksyn, O.; Schobinger-Papamantellos, P.; Ritter, C.; de Groot, C. H.; Buschow, K. H. J. *J. Alloys Compd.* **1997**, *262*−*263*, 492.

10.1021/cm051618g CCC: $30.25
Published on Web 10/07/2005

Table 1. Selected Data Collection and Refinement Parameters for the RE_2InGe_2 (RE = Sm, Gd, Tb, Dy, Ho, Yb) Ternary Compounds in the Tetragonal Space Group *P4/mbm* (No. 127)[a]

empirical formula	Sm_2InGe_2	Gd_2InGe_2	Tb_2InGe_2	Dy_2InGe_2	Ho_2InGe_2	Yb_2InGe_2
formula weight	560.70	574.50	577.84	585.00	589.86	606.08
wavelength (Å), Mo Kα			0.71073			
temperature			−153 °C			
unit cell dimensions						
a (Å)	7.3811(14)	7.3394(8)	7.3200(12)	7.2961(14)	7.2457(12)	7.199(2)
c (Å)	4.264(2)	4.2296(9)	4.1999(13)	4.169(2)	4.1541(14)	4.303(2)
c/*a*	0.5777	0.5763	0.5738	0.5714	0.5733	0.5977
volume (Å^3), $Z = 2$	232.29(11)	227.83(6)	225.04(9)	221.95(11)	218.09(9)	223.0(1)
ρ_{calc} (g/cm^3)	8.016	8.374	8.528	8.753	8.982	9.028
absorption coefficient (mm^{-1})	42.352	46.516	49.049	51.534	54.464	59.734
crystal size (mm)	0.03	0.06	0.06	0.06	0.05	0.06
	0.03	0.04	0.04	0.01	0.01	0.05
	0.02	0.04	0.03	0.01	0.01	0.03
data/parameters	176/13	177/12	170/13	169/12	169/13	165/12
R1/*w*R2 [$I > 2\sigma(I)$][b]	R1 = 0.0235	R1 = 0.0155	R1 = 0.0188	R1 = 0.0233	R1 = 0.0244	R1 = 0.0320
	*w*R2 = 0.0554	*w*R2 = 0.0376	*w*R2 = 0.0386	*w*R2 = 0.0576	*w*R2 = 0.0579	*w*R2 = 0.0701
R1/*w*R2 (all data)	R1 = 0.0299	R1 = 0.0165	R1 = 0.0196	R1 = 0.0267	R1 = 0.0283	R1 = 0.0351
	*w*R2 = 0.0570	*w*R2 = 0.0381	*w*R2 = 0.0388	*w*R2 = 0.0585	*w*R2 = 0.0586	*w*R2 = 0.0713

[a] Cell parameters reported here were determined from single-crystal X-ray diffraction. [b] $R1 = \sum||F_o| - |F_c||/\sum|F_o|$; $wR2 = [\sum[w(F_o^2 - F_c^2)^2]/\sum[w(F_o^2)^2]]^{1/2}$, where $w = 1/[\sigma^2F_o^2 + (AP)^2 + BP]$, and $P = (F_o^2 + 2F_c^2)/3$.

manides, we undertook systematic exploratory work in the RE−Ge binary systems aimed at synthesizing fully stoichiometric $REGe_2$ compounds and examination of their physical properties. It was anticipated that by employing metals with low melting points, such as In for instance (mp 156.6 °C), crystal growth of various $REGe_2$ binaries can be promoted and their structures and properties can be established reliably. The choice of In was not accidental: the In−Ge phase diagram indicates mixing in liquid state at favorable temperatures and no regions of solid solubility.[14] Moreover, there are not many ternary RE−In−Ge intermetallics, and these seem to form preferably with the early rare-earths: La_3InGe,[15] La_3In_4Ge,[15] $La_{11}In_6Ge_4$,[16a] EuInGe,[16b] RE_2InGe_2 (RE = La−Nd, Yb).[17]

Up until now, the search for novel ground states in above-mentioned binary systems proved unsuccessful. Instead, use of an In flux-growth method afforded the formation of ternary RE_2InGe_2 phases (RE = Sm, Gd−Ho, Yb), which crystallize in the tetragonal Mo_2FeB_2 type, an ordered ternary variant of the U_3Si_2 structure.[11] These ternaries are isostructural with the recently reported RE_2InGe_2 phases (RE = La−Nd, Yb) prepared through arc-melting and annealing methods.[17] Herein, we report the results of these comprehensive studies, which comprise single-crystal and powder X-ray diffraction studies and temperature- and field-dependent dc magnetization, electrical resistivity, and calorimetry measurements. The structural trends across the RE−In−Ge systems and the evolution of the magnetic properties are also discussed.

Experimental Section

Synthesis. All starting materials were stored and handled inside an Ar-filled glovebox with controlled oxygen and moisture levels below 1 ppm. Rare-earth metals (with purity >99.9%, Ames Laboratory or Alfa-Aesar), Ge (lump, 99.999%, Acros), and In (shot, 99.99%, Alfa-Aesar) were used as received. The elements with the desired stoichiometric ratios were loaded either in 2 cm^3 alumina crucibles (Coors) or in welded Nb containers, which were subsequently enclosed in evacuated fused silica tubes by flame sealing. Identical temperature profiles were used for all syntheses. Typical runs included a quick ramping to 1100 °C at a rate of 300 °C/h, homogenization for 1.5 h, and cooling at a rate of 30 °C/h. Large single crystals for structural studies and property measurements were grown using 10-fold excess of molten In as a solvent. These reactions were set up similarly and had to be removed from the furnaces at 500 °C for the sake of decanting the molten In flux. Further and more elaborate details on flux-growth techniques can be found elsewhere.[18]

Powder and Single-Crystal X-ray Diffraction. Full spheres of single-crystal X-ray diffraction data for all studied RE_2InGe_2 compounds were collected at −153 °C on a Bruker SMART 1000 CCD diffractometer using monochromated Mo Kα radiation. All studies were done with flux-grown crystals, which were cut to suitable for data collection dimensions (below ca. 0.06 mm^3) and were then mounted on glass fibers. The routine data collection comprised 0.5° *ω*-scans with 10 s exposure time per frame, up to a diffraction angle $2\theta_{max} \sim 57°$. Intensity data were collected using the SMART software[19] and were corrected for polarization effects and integrated using SAINT.[20] SADABS was used for absorption correction.[21] Details on the data collection and structure refinements for all six compounds are given in Table 1.

Structures were solved and refined on F^2 with the aid of the SHELXS and SHELXTL, respectively.[22] The tetragonal Mo_2FeB_2 structure type, an ordered ternary version of the U_3Si_2 structure,[11] served as a model for the final refinements with RE's at the *4h* Wyckoff site, In at the *2a* Wyckoff site, and Ge at the *4g* Wyckoff site, respectively (Table 2). Important bond distances are listed in Table 3. Further information in the form of combined CIF is available as Supporting Information and has also been deposited with Fachinformationzentrum Karlsruhe, 76344 Eggenstein-Le-

(14) Massalski, T. B. *Binary Alloy Phase Diagrams*; American Society for Metals: Metals Park, OH, 1990.
(15) Guloy, A. M.; Corbett, J. D. *Inorg. Chem.* **1996**, *35*, 2616.
(16) a) Mao, J.; Guloy, A. M. *J. Alloys Compd.* **2001**, *322*, 135. (b) Mao, J.-G.; Goodey, J.; Guloy, A. M. *Inorg. Chem.* **2002**, *41*, 931.
(17) a) Zaremba, V. I.; Kaczorowski, D.; Nychyporuk, G. P.; Rodewald, U. C.; Pöttgen, R. *Solid State Sci.* **2004**, *6*, 1301. (b) Zaremba, V. I.; Tyvanchuk, Y. B.; Stepien-Damm, J. *Z. Kristallogr. NCS* **1997**, *212*, 291.
(18) Canfield, P. C.; Fisk, Z. *Philos. Mag.* **1992**, *B65*, 1117.
(19) SMART NT Version 5.05, Bruker Analytical X-ray Systems, Inc., Madison, WI, 1998.
(20) SAINT NT Version 6.22, Bruker Analytical X-ray Systems, Inc., Madison, WI, 2001.
(21) SADABS NT Version 2.05, Bruker Analytical X-ray Systems, Inc., Madison, WI, 1998.
(22) (a) SHELXS-97, Bruker Analytical Systems, Inc., Madison, WI, 1990. (b) SHELXTL Version 6.10, Bruker Analytical X-ray Systems, Inc., Madison, WI, 2001.

Table 2. Atomic Coordinates and Equivalent Displacement Parameters (U_{eq}) for RE_2InGe_2 (RE = Sm, Gd, Tb, Dy, Ho, Yb)[a]

atom	*x*	*y*	*z*	U_{eq} (Å^2)[b]
Sm	0.17864(8)	$x + 1/2$	$1/2$	0.0051(3)
In	0	0	0	0.0074(4)
Ge	0.3799(2)	$x + 1/2$	0	0.0054(4)
Gd	0.17858(5)	$x + 1/2$	$1/2$	0.0044(2)
In	0	0	0	0.0074(3)
Ge	0.3791(1)	$x + 1/2$	0	0.0050(3)
Tb	0.17836(5)	$x + 1/2$	$1/2$	0.0049(2)
In	0	0	0	0.0076(3)
Ge	0.3787(1)	$x + 1/2$	0	0.0057(3)
Dy	0.17813(6)	$x + 1/2$	$1/2$	0.0066(3)
In	0	0	0	0.0083(4)
Ge	0.3785(2)	$x + 1/2$	0	0.0067(4)
Ho	0.17773(8)	$x + 1/2$	$1/2$	0.0057(3)
In	0	0	0	0.0109(5)
Ge	0.3750(2)	$x + 1/2$	0	0.0066(5)
Yb	0.1748(1)	$x + 1/2$	$1/2$	0.0053(4)
In	0	0	0	0.0103(6)
Ge	0.3771(3)	$x + 1/2$	0	0.0053(6)

[a] The Wyckoff sites occupied are *4h*, *2a*, and *4g* for RE, In, and Ge, respectively. [b] U_{eq} is defined as one-third of the trace of the orthogonalized U_{ij} tensor.

Table 3. Selected Bond Lengths (Å) for RE_2InGe_2 (RE = Sm, Gd, Tb, Dy, Ho, Yb)

Sm_2InGe_2		Gd_2InGe_2		Tb_2InGe_2	
Ge−Ge	2.508(3)	Ge−Ge	2.510(2)	Ge−Ge	2.512(2)
Ge−In	2.941(1) × 2	Ge−In	2.9204(6) × 2	Ge−In	2.910(7) × 2
Sm−Ge	2.993(1) × 2	Gd−Ge	2.9671(9) × 2	Tb−Ge	2.951(1) × 2
Sm−Ge	3.098(1) × 4	Gd−Ge	3.0794(6) × 4	Tb−Ge	3.0653(7) × 4
Sm−In	3.4511(7) × 4	Gd−In	3.4286(4) × 4	Tb−In	3.4143(5) × 4
Sm−Sm	3.8380(8) × 4	Gd−Gd	3.8165(5) × 4	Tb−Tb	3.8073(7) × 4
Sm−Sm	3.729(2)	Gd−Gd	3.707(1)	Tb−Tb	3.693(1)

Dy_2InGe_2		Ho_2InGe_2		Yb_2InGe_2	
Ge−Ge	2.508(3)	Ge−Ge	2.511(4)	Ge−Ge	2.504(5)
Ge−In	2.9002(9) × 2	Ge−In	2.876(1) × 2	Ge−In	2.855(1) × 2
Dy−Ge	2.936(1) × 2	Ho−Ge	2.918(2) × 2	Yb−Ge	2.978(2) × 2
Dy−Ge	3.0490(9) × 4	Ho−Ge	3.033(1) × 4	Yb−Ge	3.060(1) × 4
Dy−In	3.3985(7) × 4	Ho−In	3.3800(6) × 4	Yb−In	3.4193(8) × 4
Dy−Dy	3.7958(8) × 4	Ho−Ho	3.7709(7) × 4	Yb−Yb	3.7587(9) × 4
Dy−Dy	3.676(1)	Ho−Ho	3.644(2)	Yb−Yb	3.558(2)

opoldshafen, Germany (Fax: (49) 7247−808−666. E-mail: crysdata@fiz.karlsruhe.de), depository numbers CSD 415607 for Sm_2InGe_2, CSD 415608 for Gd_2InGe_2, CSD 415609 for Tb_2InGe_2, CSD 415610 for Dy_2InGe_2, CSD 415611 for Ho_2InGe_2, and CSD 415612 for Yb_2InGe_2, respectively.

X-ray powder diffraction patterns were collected on a Philips X′Pert diffractometer with monochromated Cu Kα radiation (λ = 1.5406 Å) at room temperature. Typical runs included $\theta-\theta$ scans ($2\theta_{max} = 80°$) with intervals of 0.02° and 10 s counting time. Data processing was accomplished with JADE 6.5 software,[23] and all lattice parameters refined from the powder patterns were in excellent agreement with the ones determined from single crystal work (Table 1).

Physical Property Measurements. Field-cooled and zero-field cooled dc magnetization measurements were performed for all title compounds using a Quantum Design MPMS SQUID magnetometer. The measurements were completed in the temperature range from 5 to 300 K and in a magnetic field of 0.05 T. The samples were secured in a custom-designed low background sample holder. Several specimens from different reaction batches were measured in order to provide reproducible results. In all cases, the measured material was prepared by selecting flux-grown crystals, and the phase purity was subsequently verified by taking powder X-ray diffraction patterns. Field dependence measurements up to a field of 5 T were also completed at temperatures below the magnetic ordering transition, typically 5 K.

(23) JADE Version 6.5, Materials Data, Inc., Livermore, CA, 2003.

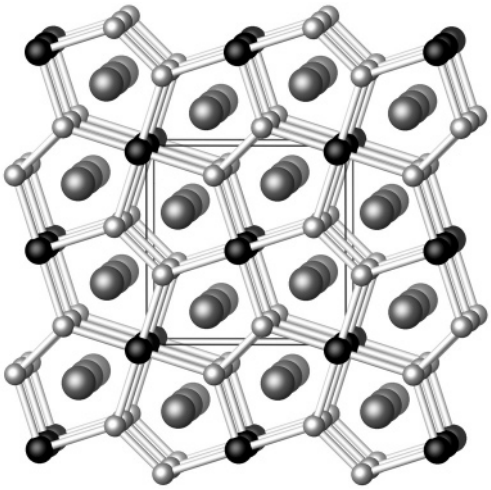

Figure 1. A perspective view of the structure of the RE_2InGe_2 (RE = Sm, Gd, Tb, Dy, Ho, Yb) compounds, viewed down the *c*-axis. Rare-earth cations are drawn as large gray spheres, the Ge atoms are drawn as small gray spheres, and In atoms are shown as black spheres, respectively. The unit cell is outlined.

The electrical resistivity and heat capacity measurements were carried out on a Quantum Design PPMS system. The resistance was measured using a four-probe technique from 2 to 300 K with excitation current of 1 mA. The ohmic contacts were made with silver epoxy. Calorimetry data for the same specimens were taken using the thermal relaxation technique. For all measurements reported herein, flux-grown single crystals were used. These were needle-shaped, with needle-axis presumed to be parallel to the direction of the crystallographic *c*-axis.

Results and Discussion

Synthesis, Structure, and Bonding. All of the title compounds crystallize with the Mo_2FeB_2 type, an ordered ternary variant of the tetragonal U_3Si_2 structure.[11] Many of the important features and crystallographic details of this structure type have been reviewed recently.[24] Therefore, only a concise description in the context of this work will be given here.

The crystal structure of the RE_2InGe_2 phases (RE = Sm, Gd−Ho, Yb) can be viewed as flat, infinite $InGe_2$ layers that are stacked above one another along the direction of the *c*-axis, with layers of rare-earth cations between them (Figure 1). Tables 2 and 3 list the positional and thermal displacement parameters and important bond distances, respectively. All Ge−Ge interatomic distances fall in the narrow range from 2.504(5) to 2.512(2) Å and compare well with those reported for the isostructural RE_2TGe_2 (T = Mg, In) phases.[17,25] Comparable Ge−Ge contacts are observed in many binary RE−germanides with 2D- and 3D-networks, including the Zintl phase $EuGe_2$,[26] where the formally reduced Ge's are connected via slightly longer distances of ca. 2.56 Å. Comparison of the Ge−Ge distances among the

(24) Lukachuk, M.; Pöttgen, R. *Z. Kristallogr.* **2003**, *218*, 767.
(25) Choe, W.; Miller, G.; Levin, E. *J. Alloys Compd.* **2001**, *329*, 121.
(26) Bobev, S.; Bauer, E. D.; Thompson, J. D.; Sarrao, J. L.; Miller, G. J.; Eck, B.; Dronskowski, R. *J. Solid State Chem.* **2004**, *177*, 3545.

reported six crystal structures does not provide evidence for systematic variation and/or correlation with the decreasing of the unit cell volume when moving across the series (Table 1).

The Ge_2 pairs are interconnected to form flat $InGe_2$ layers via four-coordinated In atoms (Figure 1), which exhibit a unique coordination environment for a group 13 element, square-planar. The In−Ge distances from 2.855(1) to 2.941(1) Å are almost 11−14% larger than the sum of the corresponding Pauling's covalent radii (2.57 Å).[27] Noteworthy, these distances are also much longer than the ones observed in EuInGe, 2.76 Å,[16b] but compare well with the In−Ge distances in La_3In_4Ge, for example.[15] The RE−In interactions appear very weak as well, as evidenced from the long RE−In contacts (Table 3). All of the above can then explain the 40−50% larger and more diffuse atomic displacement parameter (ADP) for the In atoms in all discussed structures (Table 2). The In's ADP is larger in virtually all directions and provides no evidence for disorder of any kind. The same holds true for all atoms occupying the same Wyckoff site (*2a*) in isostructural phases.[17,24,25] Despite that, the In−Ge interactions are not weak and are expected to create fairly large contributions to the total DOS near the Fermi level, as demonstrated with tight-binding LMTO-ASA band calculations for the Mg−Ge interactions in the closely related Gd_2MgGe_2 compound.[25]

Another remarkable feature of the RE_2InGe_2 (RE = Sm, Gd−Ho, Yb) structure is the 10-coordinate (pentagonal prism) geometry around the RE atoms, as shown in Figure 2a. A projection of the RE subnetwork, which comprises planar layers stacked along the *c*-axis, is shown in Figure 2b. The distances between the RE atoms within the planes, given in Table 3, are slightly longer than the sum of the corresponding metallic radii,[27] while the RE−RE interactions between the planes are significantly, ca. 12−18%, longer. These weaker layer-to-layer interactions could give rise to the antiferromagnetic ordering observed at low temperatures (below). A possible mechanism for that would involve ferromagnetic coupling of the f-electrons within the layers (shorter RE−RE distances), while the layers are antiferromagnetically coupled between each other (longer RE−RE distances). Studies on the band structure of the isostructural Gd_2MgGe_2 support such a model and suggests nearly optimized RE−RE, RE−Ge, and RE−Mg (or In) interactions in this structure.[25]

Analysis of the bonding distances in Gd_2MgGe_2 and the related RE_2InGe_2 compounds implies that structure rationalization can be approached from a different point of view, using the classic Zintl formalism.[28] It can provide an overly simplistic, yet not unrealistic electron count: since Ge with one covalent bond needs three extra electrons to complete its valence shell, the formal oxidation state for Ge in that structure would be "−3", which leaves two electrons per formula unit in the conduction band, i.e. $(Gd^{3+})_2(Mg^{2+})(Ge^{3-})_2(e^-)_2$.[25] Following the same formalism, the structures of the In-counterparts can be rationalized as $(RE^{3+})_2(In^{3+})(Ge^{3-})_2(e^-)_3$, i.e. metals with three electrons per formula unit in the conduction band. Hence, the In-containing phases will likely be better conductors than the corresponding Mg analogues because of the higher DOS at the Fermi level. Indeed, the temperature dependence of the resistivity for some of the RE−In−Ge compounds shows typical metallic behavior with low residual resistivity (below).

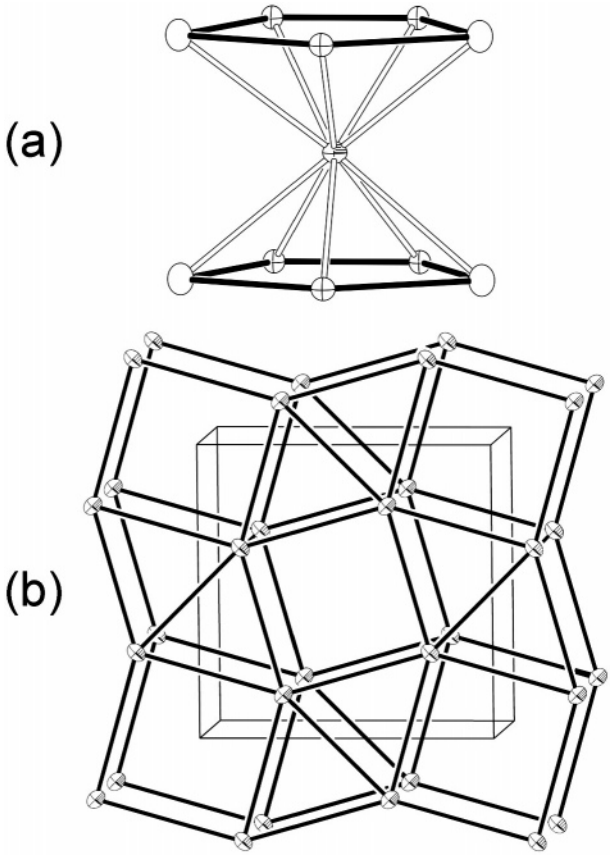

Figure 2. (a) Coordination polyhedron around the RE cations and (b) [001] projection of the RE subnetwork in RE_2InGe_2 (RE = Sm, Gd, Tb, Dy, Ho, Yb). The RE atoms are shown with full thermal ellipsoids, Ge atoms are shown with crossed ellipsoids, and In atoms are shown with boundary ellipsoids, respectively, all drawn at the 99% probability level. Bond distances are listed in Table 3.

These considerations apply to all RE_2InGe_2 phases but Yb_2InGe_2, for which the magnetic measurements strongly suggest a divalent, nonmagnetic ground state. Therefore, the formula of this compound can be broken to $(Yb^{2+})_2(In^{3+})(Ge^{3-})_2(e^-)$, with just one extra electron per formula unit. The different electronic state for the latter is clearly supported by the change of the unit cell constants (Figure 3). The unit cell volumes of the isostructural RE_2InGe_2 (RE = Sm, Gd−Ho) compounds monotonically decrease, following the Shannon cationic radii for RE^{3+} when moving across the lanthanide series.[29] Yb_2InGe_2, on the other hand, violates this trend and its larger cell volume correlates well with the Shannon cationic radius for Yb^{2+}, respectively. Interestingly, while the cell volume and the *c* lattice parameter for Yb_2InGe_2 are larger and support the arguments in favor of divalent Yb, the *a* lattice parameter seems to follow the *f*-shell contraction

(27) Pauling, L. *The Nature of the Chemical Bond*; Cornell University Press: Ithaca, NY, 1960.

(28) a) Zintl, E. *Angew. Chem.* **1939**, *52*, 1. (b) Kauzlarich, S. M. (Ed.) *Chemistry, Structure and Bonding of Zintl Phases and Ions*; VCH Publishers: New York, 1996 and the references therein.

(29) Shannon, R. D. *Acta Crystallogr.* **1976**, *A 32*, 751.

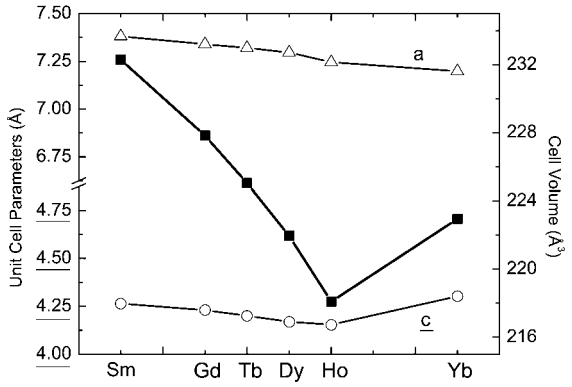

Figure 3. Plot of the measured unit cell parameters (Å) and cell volumes (Å^3) for RE_2InGe_2 (RE = Sm, Gd, Tb, Dy, Ho, Yb). Cell parameters are shown with open symbols (left *y*-axis) and the cell volume with filled symbols (right *y*-axis).

(Figure 3). Thus, the corresponding Yb−In and Yb−Ge distances, as expected, are longer than the corresponding ones in all other RE_2InGe_2 (RE = Sm, Gd−Ho) compounds (Table 3). The Yb−Yb contacts, however, are shorter than the related RE−RE distances (Table 3). All of the above suggests that the Zintl reasoning provides only a quantitative description, and that the bonding patterns in the seemingly simple RE_2InGe_2 structures are indeed rather complicated. Similar anomaly can be found by comparing the cell constants of RE_2InGe_2 and of the isotypic RE_2MgGe_2 compounds; for any given rare-earth metal, the *a* lattice parameter is consistently smaller for RE_2MgGe_2 than for RE_2InGe_2,[30] whereas the *c* lattice parameter follows a different order: it is larger for the Mg compound than for its In counterpart. The net result is that the unit cell volumes for RE_2MgGe_2 and for RE_2InGe_2 are virtually identical, despite the fact that the size of In^{3+} is almost 7% larger than that of Mg^{2+}.[29] These effects have already been noted for the isotypes RE_2MgGe_2 and RE_2InGe_2 (RE = La, Ce, Pr, Nd) and are referred to as "electronic reasons".[17a]

Last, it is worthwhile to discuss the formation and the existence of the RE_2InGe_2 phases in a wider context. After all, there are not many rare-earth-based intermetallics with In and Ge, and this new family seems to account for more than 50% of the known RE−In−Ge ternaries.[11] As discussed already, the existence of many of the RE_2InGe_2 phases (RE = Y, La−Nd, Sm, Gd−Ho, Yb) had been established from their corresponding X-ray powder patterns.[31] Reportedly, the sample preparation involves multistep arc-melting and annealing processes with no indication of the resulting phase purity. Recently, the structures of RE_2InGe_2 (RE = La−Nd) have been confirmed from single-crystal work and their physical properties determined.[17a] Again, several synthetic steps have been utilized to prepare pure samples from stoichiometric mixtures of the corresponding elements with variable success. Our approach using In flux provides an alternative route for the synthesis of these compounds. It needs to be pointed out, however, that the yields from those flux reactions were not always quantitative and that the presence of secondary phases was detected by powder X-ray diffraction in almost all cases. The size of the isolated crystals, the yields, and the present impurities vary significantly for different rare earths and, of course, were largely dependent on the heating/cooling profiles. Most commonly, cubic $REIn_3$ phases were detected in the reaction outcome, but due to the different crystal systems, the crystal morphologies for $REIn_3$ (cubes) and RE_2InGe_2 (needles) were easily distinguishable, and crystals from the studied compounds could be hand-picked for subsequent property measurements. In the Sm−In−Ge system, in addition to the desired Sm_2InGe_2 compound (needle-like morphology), the use of In as a metal flux afforded the formation of plate-like crystals of Sm_3Ge_5 with two different structures, one in the orthorhombic Y_3Ge_5 type[11] and another one in a new hexagonal type. A closer examination of both the structural and magnetic properties for the two allotropic forms of Sm_3Ge_5 will be discussed in a forthcoming publication. In other cases, such as the Dy−In−Ge system, for example, crystals with the same appearance as Dy_2InGe_2 that turned out to be of various $DyGe_{2-x}$ binaries were always present.[12,13] "On-stoichiometry" reactions in sealed Nb tubes did not produce a pure phase either. This precluded the preparation of a pure sample for property measurements, as confirmed by powder X-ray diffraction.

In the systems La through Nd, for instance, despite all the efforts, RE_2InGe_2 compounds could not be synthesized from In flux, although they have been made using different synthetic routes.[17a] The major products of those reactions were always $REGe_{2-x}$ binary phases with the α-$ThSi_2$ structure or its variants with ordered vacancies.[12] This indicates that these binaries are more thermodynamically stable relative to RE_2InGe_2 and the flux reactions are not suitable for making the ternary phases. On the other hand, RE_2InGe_2 compounds for RE = Eu, Er, Tm, and Lu could not be prepared, neither from flux nor from stoichiometric reactions,[17a,30] which suggests that the size of the rare-earth cations, not the melting point or the electronic states, plays a critical role for the formation of RE_2InGe_2. Similar structural trends are observed in the RE_2MgGe_2 family of compounds as well.[30]

Physical Properties. Temperature dependent dc magnetization measurements were performed within the interval 5−300 K and reproducible results were confirmed on all measured phases (Figure 4). The magnetic susceptibility ($\chi = M/H$) vs temperature (T) of RE_2InGe_2 (RE = Sm, Gd, Tb, Ho) is shown in Figure 4. A concise summary of the basic magnetic characteristics is provided in Table 4. As discussed above, a pure sample of Dy_2InGe_2 could not be prepared; therefore, the taken measurements are not deemed reliable. Yb_2InGe_2, in turn, exhibits Pauli-like temperature independent paramagnetism, and the magnetization data for both are provided in the Supporting Information section.

Because of the small effective moment on Sm^{3+} (Table 4) and the significant diamagnetic core and strong van Vleck paramagnetic contributions to the magnetization, Sm_2InGe_2 does not exhibit simple magnetic behavior comparable to the other localized *f*-electrons systems. Therefore, the magnetization data (Figure 4) were fitted with the modified Curie−Weiss law $\chi(T) = \chi_0 + C/(T - \theta_p)$,[32] which resulted in $\chi_0 = 1.1 \times 10^{-3}$ emu/mol and $\theta_p = -59$ K (Figure 4).

(30) Kraft, R.; Pöttgen, R. *Montash. Chem.* **2004**, *135*, 1327.
(31) Zaremba, V. I.; S-Damm, A.; Nichiporuk, G. P.; Tyvanchuk, Yu. B.; Kalchak, Ya. M. *Crystallogr. Rep.* **1998**, *43*, 8.

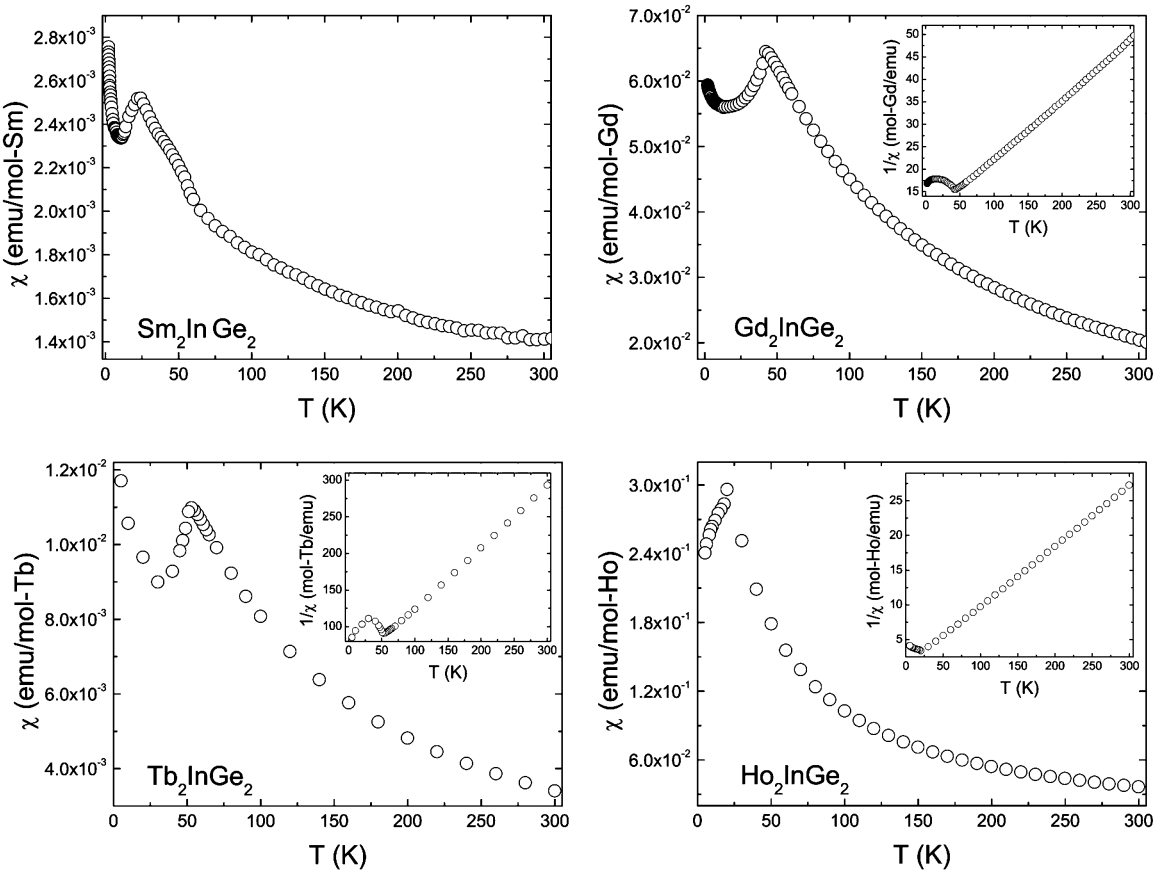

Figure 4. Magnetic susceptibility $\chi(T)$ plots for RE_2InGe_2 (RE = Sm, Gd, Tb, Ho) phases in a magnetic field of 0.05 T. Inverse magnetic susceptibility $\chi^{-1}(T)$ plots are shown in insets.

Table 4. Basic Magnetic Characteristics for the RE_2InGe_2 (RE = Sm, Gd, Tb, Ho, Yb) Compounds[a]

compound	magnetic ordering	$g\sqrt{J(J+1)}$	μ_{eff} (μ_B)	θ_p (K)	T_N (K)
Sm_2InGe_2	antiferromagnetic	0.85	0.93(5)	−59(1)	25(1)
Gd_2InGe_2	antiferromagnetic	7.94	7.72(5)	−64(1)	42(1)
Tb_2InGe_2	antiferromagnetic	9.72	9.66(5)	−49(1)	51(1)
Ho_2InGe_2	antiferromagnetic	10.61	10.30(5)	−12(1)	23(1)
Yb_2InGe_2	Pauli paramagnetic	0 (Yb^{2+})	0	n/a	n/a

[a] The constants for RE_2InGe_2 (RE = Gd, Tb, Ho) were derived by fitting the inverse susceptibility $\chi^{-1}(T)$ with a line in the temperature interval 100−300 K, whereas for Sm_2InGe_2 a nonlinear fit of the susceptibility $\chi(T)$ within 60−300 K was employed (see the text for details).

The calculated effective moment $\mu_{eff} = 0.93\ \mu_B$ is slightly higher than the expected for Sm^{3+} (Table 4). Field-dependent measurements at 5 K do not show a tendency for saturation up to magnetic field of 5 T. Reliable determination of the ordering temperature from the susceptibility data was not possible, but specific heat measurements in the range 2−50 K reveal two anomalies at approximately 26 and 15 K, respectively. These are likely indications of antiferromagnetic order; however, more measurements on larger crystals are needed to confirm it. Resistivity data taken on single crystals of Sm_2InGe_2 along the direction of the needle reveal metallic behavior (Figure 5a), with $\rho_{298} \sim 60\ \mu\Omega\cdot$cm and $\rho_2 \sim 1.2\ \mu\Omega\cdot$cm, respectively. In the antiferromagnetic state, the electrical resistivity exhibits a T^2 temperature dependence below ∼12 K.

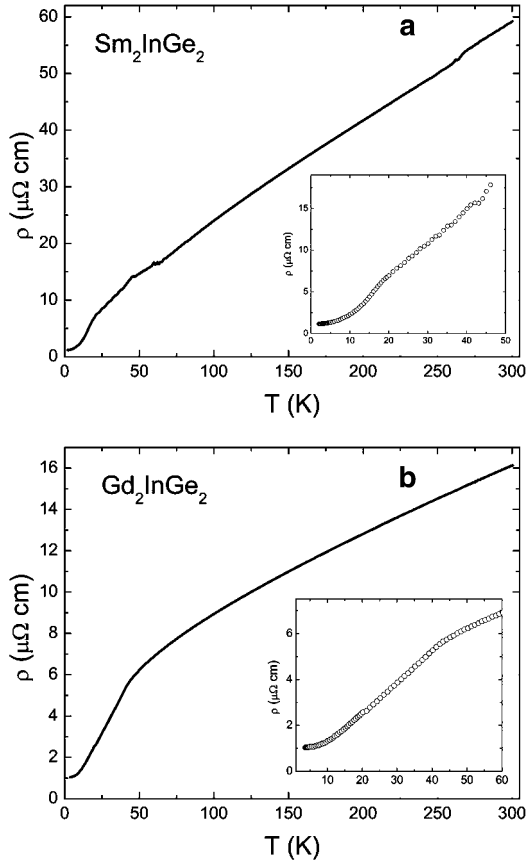

Figure 5. Resistivity $\rho(T)$ for Sm_2InGe_2 (a) and Gd_2InGe_2 (b), respectively. Insets show magnified views at low temperatures.

(32) Smart, J. S. *Effective Field Theories of Magnetism*; Saunders: Philadelphia, PA, 1966.

As seen from Figure 4, RE_2InGe_2 compounds (RE = Gd, Tb, Ho) exhibit Curie−Weiss paramagnetic behavior at temperatures above ca. 60 K. Cusplike features are visible in the data at ∼45 K for Gd_2InGe_2, ∼50 K for Tb_2InGe_2, and ∼25 K for Ho_2InGe_2, indicating the onset of long-range antiferromagnetic order in these materials. Differences in the magnetization for field-cooled and zero-field-cooled samples were marginal. The corresponding Néel temperatures (T_N) were determined from the midpoint of the jump in $d\chi/dT$, and the values are given in Table 4. These are in agreement with those expected from the de Gennes scale.[33] Above the Néel temperatures, $\chi(T)$ follows a Curie−Weiss law $\chi(T) = C/(T - \theta_p)$, where $C = N_A\mu_{eff}/3k_B$ is the Curie constant as shown in the insets of Figure 4, yielding effective moments $\mu_{eff} = 7.72\ \mu_B$ for Gd^{3+} in Gd_2InGe_2, $\mu_{eff} = 9.66\ \mu_B$ for Tb^{3+} in Tb_2InGe_2, and $\mu_{eff} = 10.30\ \mu_B$ for Ho^{3+} in Ho_2InGe_2, close to those expected (Table 4). The isothermal dependence at 5 K is almost linear with no tendency for saturation up to fields of 5 T. This behavior is in contrast with the magnetization of the isostructural RE_2InGe_2 (RE = Ce−Nd), where complex phenomena, possibly involving some spin-glass reorientations, occur.[17a]

Due to their small sizes and brittleness, single-crystals of Tb_2InGe_2 and Ho_2InGe_2 were found to be unsuitable for resistivity and calorimetry measurements, and only data for Gd_2InGe_2 are reported (Figure 5b). The data indicates metallic behavior as expected, and there is drop in the resistivity near the ordering temperature ca. 42 K. The value of the ordering temperature observed is in agreement with the value obtained from the susceptibility and heat capacity data. The change in the slope is similar to the behavior observed for the isostructural Ce_2InGe_2[17a] and is compatible with the antiferromagnetic state of the compound. The heat capacity data also shows an anomaly near 42 K, which is a clear indication of the magnetic order/disorder transition. Attempts to grow larger crystals of all RE_2InGe_2 phases are underway, and the results from the subsequent heat capacity measurements with an applied field and pressure will be published elsewhere.

Finally, as mentioned already, the structural results (Figure 3), corroborated by magnetic measurements for Yb_2InGe_2, strongly suggest divalent Yb. The temperature dependence of the magnetic susceptibility is nearly temperature independent and weakly paramagnetic and shows an impurity-contributed Curie−Weiss tail below ca. 40 K. The magnetization data were fitted with the modified Curie−Weiss law, which resulted in $\chi_0 = 6 \times 10^{-4}$ emu/mol and $\theta_p = -1.6$ K, with a calculated effective moment of $\mu_{eff} = 0.14\ \mu_B$ (see Supporting Information). This confirms the $[Xe]f^{14}$ nonmagnetic ground state for Yb in Yb_2InGe_2, with small amounts of Yb^{3+} most likely from Yb_2O_3. This is in agreement with the susceptibility data below 5 K, where at $T \sim 2.2$ K a small transition can be seen, confirming the presence of traces (below ca. 0.3 atom %) of antiferromagnetic Yb_2O_3 in the sample.[34] Similar findings are reported for many other Yb-based intermetallic compounds, and recent heat capacity measurements on $Yb_{11}GaSb_9$ confirm the presence of a thin layer of Yb_2O_3 as a result of partial surface oxidation.[35]

In that perspective and intrigued by the way the Zintl formalism accounts for the valence electron count as $(Yb^{2+})_2(In^{3+})(Ge^{3-})_2(e^-)$ with just one extra electron per formula unit—see above—we attempted the synthesis of the hereto unknown Yb_2MgGe_2 with the same structure. Following the same approach for structure rationalization, it is expected that such compound, isostructural with Yb_2InGe_2, will be charged balanced, i.e. $(Yb^{2+})_2(Mg^{2+})(Ge^{3-})_2$. These attempts have proven unsuccessful, so far, yet show a great promise, since such material may present a ground state where the trivalent $[Xe]f^{13}$ and divalent $[Xe]f^{14}$ configurations of Yb are close in energy, resulting in intermediate-valence. If that holds true, small changes in the crystallographic and electronic environment of the Yb cations (like doping) could have a remarkable effect on the physical properties, and interesting physics could result.

Conclusions

Single-crystals of six ternary RE_2InGe_2 phases for the lanthanide elements RE = Sm, Gd, Tb, Dy, Ho, and Yb were grown using an excess of indium as a flux. The compounds were systematically studied by means of X-ray diffraction, magnetometry, calorimetry, and conductivity measurements. It was found that the size of the rare-earth cation, not melting points, oxidation states, or ionization potentials, plays a decisive role for the formation of these ternary phases. At room temperature and down to ca. 60 K, the RE_2InGe_2 (RE = Sm, Gd, Tb, Ho) phases are magnetically disordered. At lower temperatures, these materials order antiferromagnetically, whereas magnetization measurements on Yb_2InGe_2 confirm Pauli-paramagnetic behavior with an effective moment of 0. The inability to prepare pure samples of Dy_2InGe_2 either by direct fusion of the corresponding elements or by flux methods precluded the unequivocal property measurements for that system. Nevertheless, preliminary magnetic susceptibility data as a function of temperature indicate ferromagnetically ordered ground state below ca. 75 K (Supporting Information), which appears to have no precedent, as no ferromagnetic behavior has been reported for any known Dy−Ge and/or Dy−In intermetallics.[12,13,36] Currently, more comprehensive work on the Dy−In−Ge system is under way.

Acknowledgment. S.B. acknowledges financial support from the University of Delaware Research Foundation (UDRF) and from the University of Delaware through a start-up grant.

Supporting Information Available: An X-ray crystallographic file for the six structures in CIF format, along with magnetization data $\chi = M/H$ vs temperature T of Yb_2InGe_2 and Dy_2InGe_2. This material is available free of charge via the Internet at http://pubs.acs.org.

CM051618G

(33) de Gennes, P. G. *J. Phys. Radium* **1962**, *23*, 510.
(34) Li, H.; Wu, C. Y.; Ho, J. C. *Phys. Rev. B* **1994**, *49*, 1447.
(35) Bobev, S.; Fritsch, V.; Thompson, J. D.; Sarrao, J. L.; Eck, B.; Dronskowski, R.; Kauzlarich, S. M. *J. Solid State Chem*. **2005**, *178*, 1071.
(36) a) Galéra, R. M.; Sole, E.; Amara, M.; Morin, P.; Burlet, P.; Murani, A. P. *J. Phys.: Condens. Matter* **2003**, *15*, 6269. (b) Gamari-Seale, H.; Anagnostopoulos, T. *J. Appl. Phys.* **1979**, *50*, 434. (c) Buschow, K. H. J.; Schobinger-Papamantellos, P.; Fischer, P. *J. Less-Common Met.* **1988**, *139*, 221.